A primer on experimental and computational rheology with fractional viscoelastic constitutive models

Citation: Ferrás, Luís Lima, Neville John Ford, Maria Luísa Morgado, Magda Rebelo, Gareth Huw McKinley, and João Miguel Nóbrega. "A Primer on Experimental and Computational Rheology with Fractional Viscoelastic Constitutive Models" (2017). AIP Conference Proceedings 1843, 26-27 July, 2017, Zlín, Czech Republic, AIP Publishing, 2017. © 2017 Authors

As Published: http://dx.doi.org/10.1063/1.4982977

Publisher: AIP Publishing

Persistent URL: http://hdl.handle.net/1721.1/119861

Version: Final published version: final published article, as it appeared in a journal, conference proceedings, or other formally published context

A primer on experimental and computational rheology with fractional viscoelastic constitutive models

Luís Lima Ferrás, Neville John Ford, Maria Luísa Morgado, Magda Rebelo, Gareth Huw McKinley, and João Miguel Nóbrega

Citation: AIP Conference Proceedings **1843**, 020002 (2017); doi: 10.1063/1.4982977
View online: http://dx.doi.org/10.1063/1.4982977
View Table of Contents: http://aip.scitation.org/toc/apc/1843/1
Published by the American Institute of Physics

A Primer on Experimental and Computational Rheology with Fractional Viscoelastic Constitutive Models

Luís Lima Ferrás[1,2 a)], Neville John Ford[2, b)], Maria Luísa Morgado[3, c)], Magda Rebelo[4, d)], Gareth Huw McKinley[5, e)], João Miguel Nóbrega[1, f)]

[1]*IPC/i3N - Institute Polymers and Composites, Department of Polymer Engineering, University of Minho, Campus de Azurém, 4800-058 Guimarães, Portugal.*
[2]*Department of Mathematics, University of Chester, CH1 4BJ, UK.*
[3]*Centro de Matemática, Polo CMAT-UTAD, Departamento de Matemática, Universidade de Trás-os-Montes e Alto Douro, UTAD, Quinta de Prados 5001-801, Vila Real, Portugal.*
[4]*Centro de Matemática e Aplicações (CMA) and Departamento de Matemática, Faculdade de Ciências e Tecnologia, Universidade NOVA de Lisboa, Quinta da Torre, 2829-516 Caparica, Portugal.*
[5]*Department of Mechanical Engineering, Massachusetts Institute of Technology, Cambridge, MA 02139 USA*

[a)]Corresponding author: luis.ferras@dep.uminho.pt
[b)]njford@chester.ac.uk
[c)]luisam@utad.pt
[d)]msjr@fct.unl.pt
[e)]gareth@mit.edu
[f)]mnobrega@dep.uminho.pt

Abstract. This work presents a brief introduction to fractional calculus and its application to some problems in rheology. We present two different viscoelastic models based on fractional derivatives (the Fractional Maxwell Model – FMM and the Fractional Viscoelastic Fluid – FVF) and discuss their reduction to the classical Newtonian and Maxwell fluids. A third model is also studied (an extension of the FMM to an invariant form), being given by a combination of the K-BKZ integral model with a fractional memory function which we denote the Fractional K-BKZ model. We discuss and illustrate the ability of these models to fit experimental data, and present numerical results for simple stress relaxation following step strain and steady shearing.

INTRODUCTION: FRACTIONAL CALCULUS AND VISCOELASTICITY

In the last few decades, a special class of viscoelastic models has drawn the attention of both engineers and mathematicians. These models make use of fractional derivatives (integro-differential operators), instead of the classical integer-order derivative and classical integral operators. The reason for such success comes from the fact that these fractional operators naturally generalize the differential equations governing important physical processes (especially processes with memory), improving their range of applicability in quantitatively describing data [1,2].

The simplest model that considers both viscous and elastic behavior is the linear Maxwell model [3], $\boldsymbol{\sigma}+\lambda\, d\boldsymbol{\sigma}/dt = \eta\dot{\boldsymbol{\gamma}}$ with $\boldsymbol{\sigma}$ the stress tensor, $\dot{\boldsymbol{\gamma}} = (\nabla u + (\nabla u)^{\mathrm{T}})$ the rate of deformation tensor, $\mathbf{u}$ the velocity vector, λ the relaxation time of the fluid and η the zero shear rate viscosity. This model can also be written in integral form as

$$\boldsymbol{\sigma}(t) = \int_0^t G_0 e^{-(t-t')/\lambda} \frac{d\boldsymbol{\gamma}}{dt'} dt', \tag{1}$$

Novel Trends in Rheology VII
AIP Conf. Proc. 1843, 020002-1–020002-13; doi: 10.1063/1.4982977
Published by AIP Publishing. 978-0-7354-1513-3/$30.00

where $G(t) = G_0 e^{-t/\lambda}$ is the relaxation modulus (the response of the stress to a step in deformation at time $t' = 0$), which exhibits an exponential decay, $\boldsymbol{\gamma}$ is the deformation tensor, and it is assumed that the fluid is at rest for $t < 0$. To represent the mechanical equivalent of this model we can assume a spring (elasticity) connected to a dashpot (viscosity), in series, with both elements subjected to the same stress, as shown in Fig. 1(a) below.

The Maxwell-Debye relaxation of stress (exponential decay) is quite common, but there are other materials showing different types of fading memory, such as an algebraic or power law decay $G(t) \sim t^{-\alpha}$, $0 < \alpha < 1$ [4,5]. If we assume the relaxation modulus for an arbitrary loading history in such materials is given by $G(t-t') = \mathbb{V}(\Gamma(1-\alpha))^{-1}(t-t')^{-\alpha}$, then we have that:

$$\boldsymbol{\sigma}(t) = \frac{1}{\Gamma(1-\alpha)} \int_0^t \mathbb{V}(t-t')^{-\alpha} \frac{d\boldsymbol{\gamma}}{dt'} dt' . \tag{2}$$

By recognizing that the Caputo fractional derivative of a general function $\boldsymbol{\gamma}(t)$ (in our case $\boldsymbol{\gamma}(t)$ is the deformation), is defined as [1,6]:

$$\frac{d^\alpha \boldsymbol{\gamma}(t)}{dt^\alpha} = \frac{1}{\Gamma(1-\alpha)} \int_0^t (t-t')^{-\alpha} \frac{d\boldsymbol{\gamma}}{dt'} dt' , \tag{3}$$

we obtain a generalized viscoelastic model [7,8], that can be written in the simple compact form:

$$\boldsymbol{\sigma} = \mathbb{V} \frac{d^\alpha \boldsymbol{\gamma}(t)}{dt^\alpha}, \ 0 < \alpha < 1 , \tag{4}$$

with a mechanical equivalent shown in Fig. 1(b). This model provides a generalized viscoelastic response, in the sense that when $\alpha = 1$ we obtain a Newtonian fluid, and when $\alpha = 0$ we obtain a Hookean elastic solid.

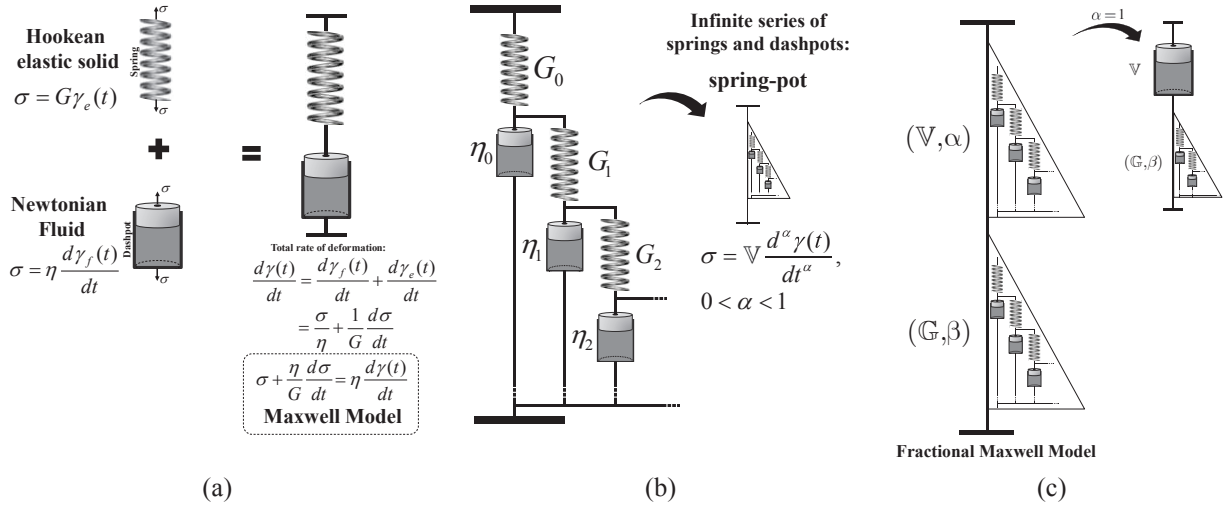

FIGURE 1. (a) A series combination of a spring and dashpot (total deformation is equal to the sum of the deformation obtained from the spring and the dashpot; the stress felt by each element is the same) – **classical Mawell Model**; (b) Series combination of springs and dashpots [7] – **Springpot**; (c) Combination of two springpots in series gives the – **Fractional Maxwell Model**. If $\alpha = 1$ we obtain the **Fractional Viscoelastic fluid**, a series combination of a springpot with a dashpot.

For specific conditions it is possible to obtain an algebraic relation between relationship $\mathbb{V}$ and $\eta_i, G_i,\ i=1,2,...$ as shown by Schiessel and Blumen [9], for the particular case of *n*-1 dashpots and *n* springs, where the last element on the right (Fig. 1(b)) is a spring with relaxation modulus G_n. The finite arrangement shows a solidlike long-time behavior, and that relation is given by:

$$\mathbb{V}=\eta_0^{\alpha}G_0^{1-\alpha} \tag{5}$$

with:

$$\frac{G_1}{\eta_0}=(-\xi)c_0;\ \frac{G_1}{\eta_1}=\frac{1(1+\xi)c_0}{1\cdot 2};\frac{G_2}{\eta_1}=\frac{1(1-\xi)c_0}{2\cdot 3};\frac{G_2}{\eta_2}=\frac{2(2+\xi)c_0}{3\cdot 4};\frac{G_3}{\eta_2}=\frac{2(2-\xi)c_0}{4\cdot 5}\ldots\frac{G_{n-1}}{\eta_{n-1}}=\frac{(n-1)((n-1)+\xi)c_0}{(2n-3)\cdot(2n-2)};\frac{G_n}{\eta_{n-1}}=\frac{(n-1)((n-1)-\xi)c_0}{(2n-2)\cdot(2n-1)}$$

where $\xi=\alpha-1$ and $c_0=G_0/\eta_0$. Notice that to obtain a relative error smaller than 0.01 with the relation given by Eq. 5, the time range should be limited to $t\in\left[100^{1/\alpha}/c_0,\ n^2/(10c_0)\right]$ [9]. Moreover, by increasing the number of elements, *n,* the time range of the above relation validity is enlarged.

Note that so far nothing has been specified regarding the choice of $\mathbb{V}(\Gamma(1-\alpha))^{-1}$ as our new algebraic relaxation modulus. The parameter $\mathbb{V}$ is a constant (for a fixed α), and is known as a quasiproperty [10]. It is best viewed as the numerical measure of a dynamical process rather than a simple material property. $\mathbb{V}(\Gamma(1-\alpha))^{-1}$ was chosen for our algebraic relaxation modulus, because in this way a generalized fractional derivative is obtained, as shown in Eq. 3, whose properties are well documented in the literature [1]. This generalization can be easily understood if we recall the following formula for the *n*-fold integral of a generic function $f(t)$,

$$\underbrace{\int_a^t\int_a^t\ldots\int_a^t f(t)\,dtdt\ldots dt}_{n\ times}=J_a^n f(t)=\frac{1}{(n-1)!}\int_a^t(t-t')^{n-1}f(t')\,dt'. \tag{6}$$

An obvious generalization to non-integer n can be performed using the Euler Gamma function $\Gamma(x):=\int_0^{\infty}t^{x-1}e^{-t}dt$, with $(n-1)!=\Gamma(n)$ for $n\in\mathbb{N}$. This leads to the Riemann-Liouville fractional integral,

$$J_a^n f(t)=\frac{1}{\Gamma(\alpha)}\int_a^t(t-t')^{\alpha-1}f(t')\,dt', \tag{7}$$

where we have used α to represent the generalization of n to non-integer values. A fractional derivative of any order can then be obtained by manipulating the number of integrations and differentiations of the function $f(t)$. By performing the $m-\alpha$ - fold integration of the m^{th} derivative of $f(t)$, $J_a^{m-\alpha}D^m f(t)$ with $m=\lceil\alpha\rceil$, we arrive at the generalized derivative formula (Caputo fractional derivative [6]) of order $m-1<\alpha<m$,

$$\frac{d^{\alpha}f(t)}{dt^{\alpha}}=\frac{1}{\Gamma(m-\alpha)}\int_a^t(t-t')^{-\alpha+m-1}\frac{d^m f(t')}{dt'^m}dt',\ \ m-1<\alpha<m. \tag{8}$$

Note that Eq. 3 is a particular case of Eq. 8 with $m=1$.

Returning to the generalized model (Fig. 1(b)) we see that its mechanical equivalent is composed of an infinite combination of springs and dashpots [7], known as a springpot [11]. Since the classical Maxwell model makes use of two elements, a spring and a dashpot in series, similarly the Fractional Maxwell Model (FMM) is the result of a combination of two linear fractional elements (springpots) in series (Fig. 1(c)). In a series configuration the stress felt by each springpot is the same, that is, $\boldsymbol{\sigma}=\mathbb{V}\,d^{\alpha}\boldsymbol{\gamma}_1(t)/dt^{\alpha}=\mathbb{G}\,d^{\beta}\boldsymbol{\gamma}_2(t)/dt^{\beta},\ 0<\alpha,\beta<1$, and the total deformation is

given by the sum of the deformation obtained for each springpot, $\boldsymbol{\gamma}(t)=\boldsymbol{\gamma}_1(t)+\boldsymbol{\gamma}_2(t)$, (Fig. 1(c)). The FMM can then be written as,

$$\boldsymbol{\sigma}(t)+\frac{\mathbb{V}}{\mathbb{G}}\frac{d^{\alpha-\beta}\boldsymbol{\sigma}(t)}{dt^{\alpha-\beta}}=\mathbb{V}\frac{d^{\alpha}\boldsymbol{\gamma}(t)}{dt^{\alpha}}, \tag{9}$$

where it was assumed (without loss of generality) that $0<\beta\le\alpha<1$.

This brief introduction to fractional calculus and the FMM is now followed by a general discussion on the properties and admissibility of the linear viscoelastic FMM in Section 2. Section 3 presents a brief discussion on the frame invariant Fractional K-BKZ formulation [2] suitable for large strains, Section 4 demonstrates the ability of fractional viscoelastic models to accurately and compactly fit experimental data, and Section 5 presents the numerical solution of a simple stress relaxation following step strain, and, steady shearing. The paper ends with the main conclusions of the work performed.

SOME PROPERTIES OF THE FMM

The FMM (Eq. 9) with $\alpha\neq1$ shows unbounded stress growth following start-up of steady shear at $\dot{\gamma}=\dot{\gamma}_0H(t)$ (with $H(t)$ the Heaviside function), that is, $\eta^+(t)=\lim_{t\to\infty}\sigma(t)/\dot{\gamma}_0$ diverges as $t^{1-\alpha}$. Therefore, it is not suitable to describe the steady flow of viscoelastic fluids. On the other hand, if we assume $\alpha=1$ (combination of a springpot and a dashpot in series as shown in Fig. 1(c)), the stress growth becomes bounded, and the model is suitable for describing the transient response of fluids. From now on, the FMM with $\alpha=1$ will therefore be referred to as the Fractional Viscoelastic Fluid model (FVF).

It is important to understand how the FMM reduces to a Newtonain fluid, an elastic solid and to the classical Maxwell model. These limiting cases can be obtained by taking the limits $\alpha\to1,\beta\to1$ (Newtonian fluid: two dashpots in series, in which case the total viscosity becomes $1/\mu=1/\mu_1+1/\mu_2$), $\alpha\to1,\mathbb{G}\to\infty$ (Newtonian fluid: one dashpot and an infinite rigid spring), $\alpha\to0,\ \beta\to0$ (elastic solid: two springs in series, so that the total modulus is $1/G=1/G_1+1/G_2$) (see Figs. 2(a) and (b)). The classical Maxwell model can be obtained when $\alpha\to1,\ \beta\to0$ as shown next. From the right-hand-side of Eq. 9, we have:

$$\lim_{\alpha\to1}\frac{d^{\alpha}\boldsymbol{\gamma}(t)}{dt^{\alpha}}=\lim_{\alpha\to1}\frac{1}{\Gamma(1-\alpha)}\int_0^t(t-t')^{-\alpha}\frac{d\boldsymbol{\gamma}}{dt'}dt', \tag{10}$$

and, making use of the formula for integration by parts $\int_a^b udv=[uv]_a^b-\int_a^b vdu$ we can obtain the limit by:

$$\begin{aligned}
\lim_{\alpha\to1}\frac{1}{\Gamma(1-\alpha)}\int_0^t(t-t')^{-\alpha}\frac{d\boldsymbol{\gamma}}{dt'}dt' &= \lim_{\alpha\to1}\frac{1}{\Gamma(1-\alpha)}\int_0^t\underbrace{\frac{d\boldsymbol{\gamma}(t')}{dt'}}_{u}d\left(\underbrace{\frac{-(t-t')^{1-\alpha}}{1-\alpha}}_{v}\right)dt' \\
&= \lim_{\alpha\to1}\frac{1}{\Gamma(1-\alpha)}\left(\left[-\frac{d\boldsymbol{\gamma}(t')}{dt'}\frac{(t-t')^{1-\alpha}}{1-\alpha}\right]_0^t-\int_0^t\frac{-(t-t')^{1-\alpha}}{1-\alpha}\frac{d^2\boldsymbol{\gamma}(t')}{dt'^2}dt'\right) \\
&= \lim_{\alpha\to1}\frac{1}{\Gamma(2-\alpha)}\left[\frac{d\boldsymbol{\gamma}(0)}{dt'}(t-0)^{1-\alpha}-\int_0^t(t-t')^{1-\alpha}\frac{d^2\boldsymbol{\gamma}(t')}{dt'^2}dt'\right] \\
&= \frac{d\boldsymbol{\gamma}(0)}{dt'}+\left[\frac{d\boldsymbol{\gamma}(t')}{dt'}\right]_0^t=\dot{\boldsymbol{\gamma}}(t)
\end{aligned} \tag{11}$$

For the left-hand-side of Eq. 9, if we follow the same procedure shown in Eq. 11 we obtain the following:

$$\lim_{\alpha-\beta\to 1}\frac{d^{\alpha-\beta}\boldsymbol{\gamma}(t)}{dt^{\alpha-\beta}}=\lim_{\beta\to 0}\frac{1}{\Gamma(\beta)}\int_0^t(t-t')^{-(1-\beta)}\frac{d\boldsymbol{\sigma}(t')}{dt'}dt'=\frac{d\boldsymbol{\sigma}(t)}{dt}. \tag{12}$$

This limit is indicated schematically in Fig. 2(b)-bottom. Assuming $\alpha\to 1$ (see Eq. 11), we can recover a Newtonian fluid by letting $\beta\to 1$:

$$\lim_{\alpha-\beta\to 1}\frac{d^{\alpha-\beta}\boldsymbol{\gamma}(t)}{dt^{\alpha-\beta}}=\lim_{\beta\to 1}\frac{1}{\Gamma(\beta)}\int_0^t(t-t')^{-(1-\beta)}\frac{d\boldsymbol{\sigma}(t')}{dt'}dt'=\left[\frac{d\boldsymbol{\sigma}(t')}{dt'}\right]_0^t=\boldsymbol{\sigma}(t)-\boldsymbol{\sigma}(0) \tag{13}$$

Note that in this case we assume the fluid is at rest in the beginning of the experiment, with $\boldsymbol{\sigma}(0)=0$ (see Fig. 2(a)-top). All the special cases that can be obtained from the FMM are illustrated in Figs. 2(a) and (b).

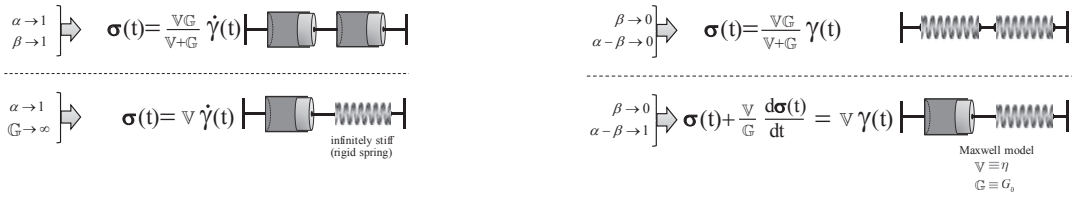

(a) (b)

FIGURE 2. Different limiting cases that can be derived from the FMM. (a) The limit $\alpha\to 1$: Newtonian fluid with either two dashpots in series (top $\beta\to 1$), or a Newtonian fluid with a dashpot and an infinite rigid spring in series (bottom $\mathbb{G}\to\infty$); (b) The limit $\beta\to 0$: gives either a Hookean solid (top) with two springs in series, classical Maxwell model (bottom).

A RHEOLOGICALLY INVARIANT FRACTIONAL K-BKZ MODEL

The FMM is a good model for describing the linear viscoelastic response of many materials, but it is not frame-invariant (as is also the case for the linear Maxwell model) [12] and therefore it is not suitable for describing the response of real materials under large deformations. In order to address this issue a few solutions have been proposed in the literature [2,13], and we will now explore the solution proposed by Jaishankar and Mckinley [2].

As we show in Section 4, the ability of the FMM to fit linear experimental data is strictly related to the form of the Mittag-Lefler function. Therefore, Jaishankar and Mckinley [2] proposed a model that is a combination of the Mittag-Leffler function with the variation of the K-BKZ [15] model proposed by Wagner, Raible and Meissner [16,17]. A similar idea was proposed by Freed and Diethelm [14] where a viscoelastic model of the K-BKZ type is combined with the standard fractional order viscoelastic solid to model biological tissue.

The model proposed by Jaishankar and Mckinley [2] (from now on referred to as the Fractional K-BKZ) is written in the general K-BKZ form as:

$$\boldsymbol{\sigma}(t)=\int_0^t m(t-t')h(I_1,I_2)\mathbf{C}_{t'}^{-1}dt', \tag{14}$$

where $\mathbf{C}^{-1}=\mathbf{F}^{-1\ T}\cdot\mathbf{F}$ is the Finger tensor ($\mathbf{F}$ is the finite deformation tensor) [18], I_1, I_2 are the traces of $\mathbf{C}^{-1}$ and $\mathbf{C}$, respectively and $h(I_1,I_2)$ is termed the *damping function* [16]. A large number of damping functions can be found in the literature (see the *Drugstore of Rheology* by D. Joseph [19] and also [17]). The term $m(t-t')$ is known as the memory function and for the Fractional K-BKZ model it was proposed in [2] to be of the form:

$$m(t-t') = \frac{dG(t-t')}{dt'} = -\mathbb{G}(t-t')^{-1-\beta} E_{\alpha-\beta,-\beta}\left(-\frac{\mathbb{G}}{\mathbb{V}}(t-t')^{\alpha-\beta}\right), \tag{15}$$

where $E_{a,b}(z)$ is the generalized Mittag-Leffer function [1] (note that here the relaxation modulus $G(t-t')$ is the one obtained for the FMM). This model was applied by [2] to describe the steady shearing flow of Xanthan gum solutions and provided a very accurate description of experimental data. For the case of steady shear flow the Finger strain tensor can be simplified to give $\dot{\gamma}_0(t-t')$ (where $\dot{\gamma}_0$ is the steady shear rate), and the model given in Eq. 14 becomes:

$$\sigma_{xy}(t) = \int_0^t m(t-t')h(\gamma)\dot{\gamma}_0(t-t')dt', \tag{16}$$

The damping function, $h(\gamma)$, was obtained from a fit to the relaxation modulus of the test materials obtained for different deformations/amplitudes. For many materials the relaxation modulus shows time-strain separability and can therefore be written in the form:

$$\frac{G(t,\gamma)}{G(t)} = \frac{G(t)h(\gamma)}{G(t)} = h(\gamma) = \frac{1}{1+a\gamma^2}, \tag{17}$$

with $a = 0.3$ for Xanthan gum solutions [2]. Note that $h(\gamma) = h(\sqrt{I_1 - 2})$ for a 2D steady shearing flow, with I_1 the first invariant of the Finger tensor. Jaishankar and Mckinley [2] showed that this model could capture well the steady shear viscosity, first normal stress difference, along other properties of polymer solutions such as Xanthan gum, by only considering the flow parameters $\mathbb{V}, \mathbb{G}, \alpha, \beta$ obtained from a FMM fit to linear data (obtained in Small Amplitude Oscillatory Shear experiments) plus one additional nonlinear parameter ($a = 0.3$) determined from the damping function, Eq. 17.

FITTING OF EXPERIMENTAL DATA – THE LINEAR REGIME

Since the FMM (Eq. 9) can describe a wide range of fluid behaviors, and also forms the basis for the Fractional K-BKZ, we tested its ability to fit the storage and loss moduli obtained for a HDPE at 190ºC [20].

As shown in Fig. 3, the quality of the fit increases with the number of parameters. To compare the quality of the different fits we have defined the total residual error $\varepsilon = \sum_i \left[\log G_i' - \log G_{fit}'(\omega_i)\right]^2 + \sum_i \left[\log G_i'' - \log G_{fit}''(\omega_i)\right]^2$.

Note that the 3 parameter FVF already provides a good quality fit (the fit for high frequencies could be improved, but at the expense of losing some quality in the fit for small frequencies), but a better fit is obtained with the FMM and the 8-mode Maxwell model. The FMM only requires 4 model parameters to describe the data, whereas the 8-mode Maxwell model requires 16. Therefore we may conclude that the FMM has a more parsimonious performance in the small amplitude oscillatory shear flows than the 8-mode Maxwell model (even though it shows an unbounded stress growth following start-up of steady shear).

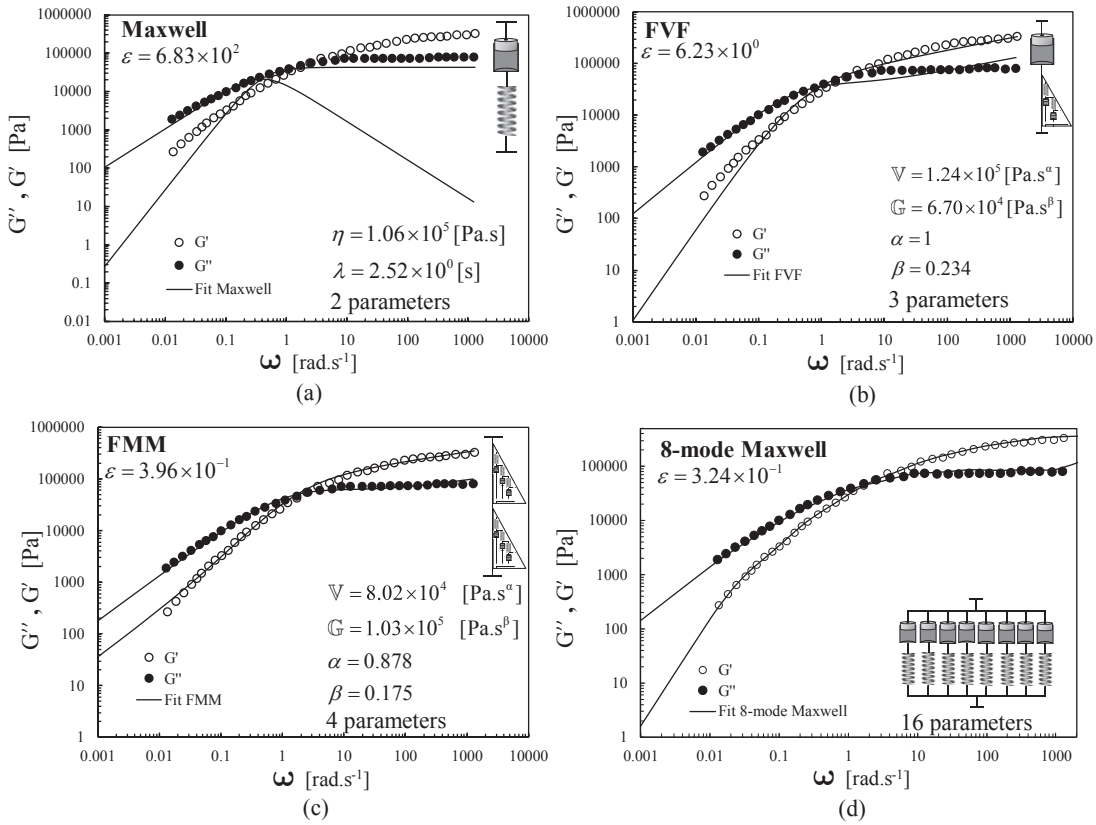

FIGURE 3. Fit of linear viscoelastic data for G' and G'' obtained for a HDPE at 190ºC [20]: (a) Maxwell model fit; (b) Fractional Viscoelastic Fluid fit; (c) Fractional Maxwell model fit; (d) 8-mode Maxwell model fit (the parameters are given in [21]).

NUMERICAL SOLUTION OF LINEAR AND NON-LINEAR SHEAR FLOWS

Although analytical and semi-analytical results exist for both models described before (FMM and Fractional K-BKZ), they are limited to specific spatially homogeneous flows due to the complexity of the integro-differential equations involved. Therefore, it is useful to develop a numerical code that can compute the behavior of such material models in more complex unidirectional and time-varying flows.

To tackle this subject using computational methods, we consider two different shear configurations, that were chosen due to the existence of an analytical solution in each case: a step-strain test for the FMM and a steady-shear test for the Fractional K-BKZ. These numerical codes do not yet allow the numerical solution of fractional models in generalized complex geometries, but, facilitate the understanding of the behavior of these fractional models in unidirectional time-varying shear flows, and, allow us to create a base of understanding for a future implementation of these models in a more general framework.

We assume the fluid under study is confined between two infinite parallel plates (see [22]), as shown in Fig. 4.

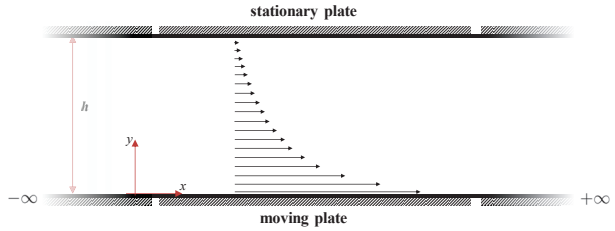

FIGURE 4. Schematic of the unidirectional shear flow geometry in which we have a stationary top plate and a moving bottom plate.

FMM Step-Strain flow

In this subsection we seek to simulate the limit of a step-strain, $\gamma(t)=\gamma_0 H(t)$, with $H(t)$ the Heaviside step function, $\gamma_0 = L/h$, and L the distance travelled by the bottom plate. For that we consider the top plate is fixed (the usual no-slip boundary condition $u(h)=0$) and that the bottom plate moves with a velocity profile (approaching a step-strain) given by (see Fig. 5(a)):

$$u(t,0)=\frac{L}{\psi\sqrt{\pi}}\exp[-((t-t_d)/\psi)^2]\,. \tag{18}$$

Note that as $\psi\to 0$, $u(t,0)$ converges to the Dirac delta function multiplied by the distance, L, traveled by the plate (assuming $t_d=0$). The finite (>0) delay time, t_d, comes from the need to have an initial condition $du(t,y)/dt=0$ at $t=0$. This is a requirement of the integro-differential equations governing this problem (this boundary condition is required when deriving analytical expressions for the stress relaxation, steady shear viscosity, etc [2]). The specification of a delay time t_d, together with ψ, allow us to get $du(t,y)/dt$ at $t=0$ to be as small as we want. This derivative converges to zero when $|t|\to\infty$ or $\psi\to 0$ (assuming $t_d>0$).

The equations governing this problem are the momentum equation [22] and the FMM constitutive equation,

$$\rho\frac{\partial u(t,y)}{\partial t}=\frac{\partial \sigma_{xy}(t,y)}{\partial y}, \tag{19}$$

$$\sigma(t,y)+\frac{\mathbb{V}}{\mathbb{G}}\frac{d^{\alpha-\beta}\sigma(t,y)}{dt^{\alpha-\beta}}=\mathbb{V}\frac{d^{\alpha}\gamma(t,y)}{dt^{\alpha}}, \tag{20}$$

with the continuity equation being verified automatically for a unidirectional shearing flow. If we apply the operation $\left(1+(\mathbb{V}/\mathbb{G})d^{\alpha-\beta}/dt^{\alpha-\beta}\right)$ to Eq. 19 and $\partial/\partial y$ to Eq. 20 we obtain the following velocity and shear stress equations:

$$\rho\left(1+\frac{\mathbb{V}}{\mathbb{G}}\frac{d^{\alpha-\beta}}{dt^{\alpha-\beta}}\right)\frac{\partial u(t,y)}{\partial t}=\frac{\mathbb{V}}{\Gamma(1-\alpha)}\int_0^t (t-t')^{-\alpha}\frac{\partial^2 u(t',y)}{\partial y^2}dt', \tag{21}$$

$$\sigma_{xy}(t,y)+\frac{\mathbb{V}}{\mathbb{G}\Gamma(1-(\alpha-\beta))}\int_0^t (t-t')^{-(\alpha-\beta)}\frac{\partial \sigma_{xy}(t',y)}{\partial t'}dt'=\frac{\mathbb{V}}{\Gamma(1-\alpha)}\int_0^t (t-t')^{-\alpha}\frac{\partial u(t',y)}{\partial y}dt'. \tag{22}$$

A numerical method (based on finite differences) used in the solution of this system of equations is explained in detail in [23] for the case of pure tangential annular flow (the differences between this case and the one shown in [23] is that in this work we take the planar limit). The mesh size used in the simulations is $\Delta y/h=2.35\times10^{-5}$ and $\Delta t_{\min}/\tau=4.5\times10^{-4}$ (with $\tau=(\mathbb{V}/\mathbb{G})^{1/(1-\beta)}$ the relaxation time of the fluid [2]). We used graded meshes when discretizing time [23]. We have used the parameters $\psi/\tau=2.68\times10^{-3}$ and $t_d/\tau=1.12\times10^{-2}$ (see Eq. 18).

Two different deformations $\gamma_0=L/h$ were considered, $\gamma_0=0.05$ and $\gamma_0=1$ (i.e. 100% strain), and the model parameters were the ones obtained for the FVF – Fig. 3(b).

The results obtained for the stress relaxation are shown in Fig. 5(b). In Figs. 5(c) and (d) we show the influence of the fractional exponents α, β. Note that the power law slope at small times is β and for long times is α, meaning that these models are suitable for describing processes with more than one relaxation time [2].

As expected the maximum stress increases with increasing strain amplitude and a convergence to the analytical solution is observed (see Fig. 5(b)). The analytical solution is given by [7,8] (we consider $\alpha=1$),

$$\frac{\sigma(t)}{\gamma_0}=G(t)=-\mathbb{G}t^{-\beta}E_{\alpha-\beta,1-\beta}\left(-\frac{\mathbb{G}}{\mathbb{V}}t^{\alpha-\beta}\right), \tag{23}$$

and is used as the relaxation function (the integral of Eq. 15) in the integral model proposed in Section 3. Note that Eq. 23 provides the appropriate normalization ($\mathbb{G}\tau^{-\beta}$) for the shear stress relaxation shown in Fig. 5(b) [2].

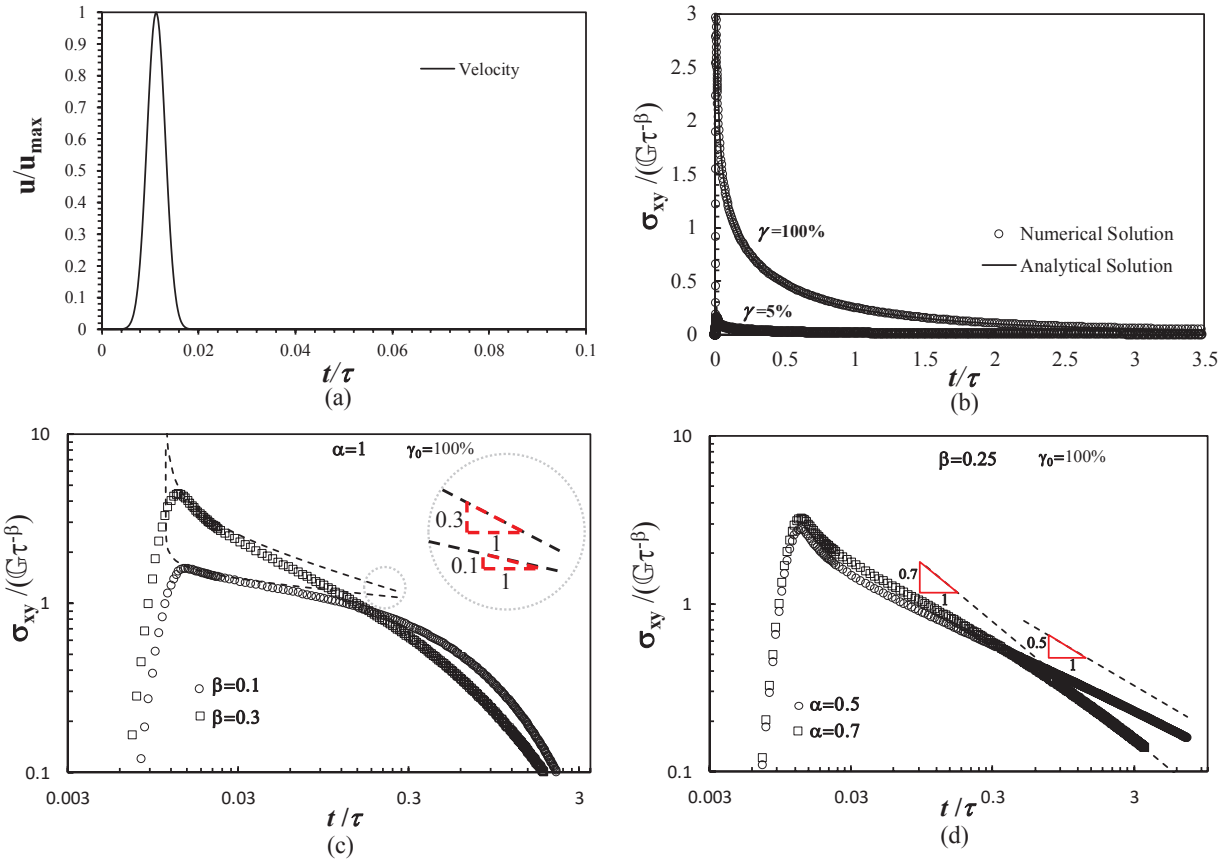

FIGURE 5. Normalized shear stress relaxation obtained for the special FVF limit (with $\alpha = 1$), ψ/τ = 2.68×10^{-3} and t_d/τ = 1.12×10^{-2}: (a) FVF with parameters shown in Fig. 3(b) and $\gamma_0 = 0.05, 1$ (the inset shows the normalized velocity profile, Eq. 18, with $u_{\max} = u(t_d, 0) = L/(\psi\sqrt{\pi})$; (b) influence of β ($\gamma_0 = 100\%$). The inset shows the slope of the normalized shear stress expected for $t \ll \tau$; (c) influence of α ($\gamma_0 = 100\%$).

The good agreement between analytical and numerical solutions supports our assertion that the numerical code is robust and can be used in the prediction of real fluid behavior, modeled both by the FVF and FMM.

The potentiality of the fractional model can be seen for the case where different fractional exponents are considered, as shown in Fig. 5(c) for a deformation of $\gamma_0 = 100\%$, and $\beta = 0.1, 0.3$. By looking at Fig. 5(c) we see that as β decreases the springpot converges to a spring (see Fig. 2) and the model starts to approach the linear Maxwell limit, that is obtained when $\alpha \to 1$ and $\beta \to 0$, and therefore, the peak of the stress is smaller, but, it takes more time to relax (smaller rate of relaxation). As we increase the value of β, the FVF evolves towards a Newtonian fluid, since each springpot converges to a dashpot when $\alpha \to 1$ and $\beta \to 1$.

Fractional K-BKZ steady-shear flow

In this subsection we seek to simulate the limit of a steady shear deformation, $\dot{\gamma}(t) = \dot{\gamma}_0 H(t)$ with $\dot{\gamma}_0 = U/h$ (U is a constant velocity imposed on the bottom plate), for a fluid modelled by the Fractional K-BKZ. For that we consider that the top plate is fixed ($u(t,h) = 0$) and that the bottom plate moves with a velocity profile given by (see Fig. 6(a)):

$$u(t,0) = \frac{U}{1+\exp(-(t-t_d)/\psi)}, \tag{24}$$

mimicking the start up if a steady shear experiment. Note that as $\psi \to 0$, and $t_d \to 0$ $u(t,0)/h$ converges to $\dot{\gamma}_0 H(t-t_d)$. For this study we have considered the HDPE material at 190ºC, described before. Since the objective is to test non-linear deformations, we considered the same damping function as the one used in [2], which showed a good fit to the experimental data for the shear viscosity up to shear rates of 1 s^{-1} (see Fig. 6(b)). A better global fit could be obtained with different values of the parameter *a*, but the fitting quality in the transition from the linear to the nonlinear behavior would decrease.

The equations governing this flow are then the momentum and Fractional K-KBKZ constitutive equations:

$$\rho \frac{\partial u(t,y)}{\partial t} = \frac{\partial \sigma_{xy}(t,y)}{\partial y}, \tag{25}$$

$$\boldsymbol{\sigma}(t,y) = \int_0^t -\mathbb{G}(t-t')^{-1-\beta} E_{\alpha-\beta,-\beta}\left(-\frac{\mathbb{G}}{\mathbb{V}}(t-t')^{\alpha-\beta}\right)\frac{1}{1+0.3(I_1-2)}\mathbf{C}_{t'}^{-1}(t,y)dt', \tag{26}$$

with the continuity equation being automatically satisfied again for this unidirectional time varying flow.

We still need another equation to track the evolution of the Finger tensor $\mathbf{C}_{t'}^{-1}(t,y)$ in time, for each $0 < t' < t$. The extra equation comes from the fact that the Finger tensor has zero upper convected derivative [24]. The evolution equation is then given by:

$$\overset{\nabla}{\mathbf{C}}_{t'}^{-1}(t,y) \equiv \frac{\partial \mathbf{C}_{t'}^{-1}(t,y)}{\partial t} + \mathbf{u}\cdot\nabla\mathbf{C}_{t'}^{-1}(t,y) - \nabla\mathbf{u}\cdot\mathbf{C}_{t'}^{-1}(t,y) - \mathbf{C}_{t'}^{-1}(t,y)\cdot(\nabla\mathbf{u})^T = 0 \tag{27}$$

where $\nabla\mathbf{u}$ is the velocity gradient tensor. Based on the flow considered in this work (Fig. 4), Eq. 27 can be further simplified and the four components of the 2D Finger tensor $\mathbf{C}_{t'}^{-1}(t,y) = \mathbf{C}_{t'}^{-1}$ can be obtained upon integration, being given by:

$$\mathbf{C}_{t'}^{-1} = \begin{bmatrix} \mathbf{C}_{t',xx}^{-1} & \mathbf{C}_{t',xy}^{-1} \\ \mathbf{C}_{t',yx}^{-1} & \mathbf{C}_{t',yy}^{-1} \end{bmatrix} = \begin{bmatrix} 1+2\int_{t'}^{t}\frac{\partial u(t'',y)}{\partial y}\left[\int_{t'}^{t''}\frac{\partial u(t''',y)}{\partial y}dt'''\right]dt'' & \int_{t'}^{t}\frac{\partial u(t'',y)}{\partial y}dt'' \\ \int_{t'}^{t}\frac{\partial u(t'',y)}{\partial y}dt'' & 1 \end{bmatrix}. \tag{28}$$

Note that to perform the integration of Eq. 27 we have used the initial condition $\mathbf{C}_{t'}^{-1}(t',y) = \mathbf{1}$, with $\mathbf{1}$ the identity matrix (meaning that there is no deformation when a new deformation field is *created* at instant t'). In this case we have a continuous evolution of all the Finger tensors for each element in the flow, and this allows us to gain knowledge on the implementation of this method in more general codes [24]. As expected, for steady shearing ($\dot{\gamma}_0$) we obtain:

$$\mathbf{C}_{t'}^{-1} = \begin{bmatrix} 1+[\dot{\gamma}_0(t-t')]^2 & \dot{\gamma}_0(t-t') \\ \dot{\gamma}_0(t-t') & 1 \end{bmatrix}, \tag{29}$$

and the first invariant $I_1 = \mathbf{tr}(\mathbf{C}_{t'}^{-1})$ becomes $I_1 = 2+[\dot{\gamma}_0(t-t')]^2$ leading to $h(\sqrt{I_1-2}) = h(\gamma)$. With some algebra the equations governing this flow can be further simplified. The momentum equation only depends on the velocity field, and, we calculate the shear stress based on this velocity field. The normal stress σ_{xx} is then calculated based on the velocity and shear stress fields. The normal stress σ_{yy} depends on the velocity field through I_1.

$$\rho \frac{\partial u(t,y)}{\partial t} = \int_0^t -\mathbb{G}(t-t')^{-1-\beta} E_{\alpha-\beta,-\beta}\left(-\frac{\mathbb{G}}{\mathbb{V}}(t-t')^{\alpha-\beta}\right)\frac{1}{1+0.3(I_1-2)}\int_{t'}^{t}\frac{\partial^2 u(t'',y)}{\partial y^2}dt''dt', \tag{30}$$

$$\sigma_{xy}(t,y)=\int_0^t -\mathbb{G}(t-t')^{-1-\beta}E_{\alpha-\beta,-\beta}\left(-\frac{\mathbb{G}}{\mathbb{V}}(t-t')^{\alpha-\beta}\right)\frac{1}{1+0.3(I_1-2)}\int_{t'}^{t}\frac{\partial u(t'',y)}{\partial y}dt''dt', \tag{31}$$

$$\sigma_{xx}(t,y)=\int_0^t -\mathbb{G}(t-t')^{-1-\beta}E_{\alpha-\beta,-\beta}\left(-\frac{\mathbb{G}}{\mathbb{V}}(t-t')^{\alpha-\beta}\right)\frac{1}{1+0.3(I_1\quad 2)}\left(1+2\int_{t'}^{t}\frac{\partial u(t'',y)}{\partial y}\left[\int_{t'}^{t''}\frac{\partial u(t''',y)}{\partial y}dt'''\right]dt''\right), \tag{32}$$

$$\sigma_{yy}(t,y)=\int_0^t -\mathbb{G}(t-t')^{-1-\beta}E_{\alpha-\beta,-\beta}\left(-\frac{\mathbb{G}}{\mathbb{V}}(t-t')^{\alpha-\beta}\right)\frac{1}{1+0.3(I_1-2)}\,dt', \tag{33}$$

This system of equations is then numerically solved (see [25] for more details) using a numerical approximation based on finite differences for the time and spatial derivatives and a discretization of the integrals with the trapezoidal rule. The boundary conditions for velocity were already presented (see Eq. 27) and we have also considered:

$$\mathbf{C}^{-1}(0,y)=\mathbf{1}. \tag{34}$$

Note that to calculate the velocity field (Eq. 29) we assume the invariant I_1 is known (from the previous iteration). The mesh size used in the simulations is $\Delta y/h=2.35\times10^{-4}$ and $\Delta t_{\min}/\tau=4.5\times10^{-4}$ (we used again graded meshes when discretizing time). We have also used the parameters $\psi/\tau=2.68\times10^{-3}$ and $t_d/\tau=1.12\times10^{-2}$.
In order to compare the numerical results with results from the literature (the semi-analytical solution presented in [2]) we numerically computed the shear stress at the upper wall (numerical solution of Eqs. 30 and 31), and calculated the shear viscosity for different shear rates with $\eta(\dot\gamma)=\sigma_{xy}(t,h)/\dot\gamma$. The numerical results are shown in Fig. 6(b), together with the experimental data gathered from [21] for the HDPE at 190ºC. We see two sets of numerical/semi-analytical results. The semi-analytical results are obtained from the formula given in Eq. 29 of [2] and the numerical results are provided by the numerical solution of Eqs. 30 and 31.

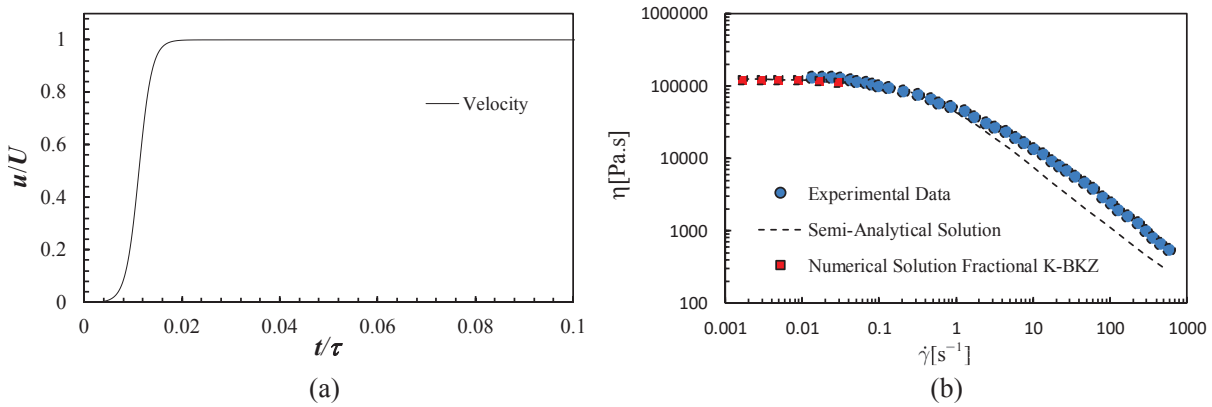

FIGURE 6. (a) Velocity profile obtained from Eq. 24. (b) Shear viscosity versus shear rate. Comparison of experimental data [20] and numerical results. The parameters used are $\mathbb{V}=1.24\times10^5\,[\text{Pa.s}^\alpha],\mathbb{G}=6.70\times10^4\,[\text{Pa.s}^\beta],\alpha=1,\beta=0.234,a=0.3$.

The numerical solution of Eqs. 30 and 31 is expensive in terms of computational time since at each instant t' a new Finger tensor is created and the past Finger tensors are not eliminated (we accumulate all the deformation along all previous times), and by using the analytical expressions for the Finger tensor (Eq. 28) we obtain a discretized nested sum. This consumes the time and memory of the computer, with the simulation becoming slower and slower as we evolve in time. This is a price we must pay to obtain an invariant model with the same linear viscoelastic properties of the FMM and FVF models (that are much easier to implement numerically). The method can be improved by numerically solving Eq. 27 to obtain the Finger tensor [24], avoiding in this way the time consuming nested sums.

CONLUSIONS

We have shown how to obtain, using fractional calculus concepts, the fractional viscoelastic models of differential and integral types. We mainly studied and compared three different models, the Fractional Viscoelastic Fluid (FVF), the Fractional Maxwell Model (FMM) and a frame-invariant K-BKZ formulation (Fractional K-BKZ). It was also demonstrated that, depending on the model parameters, the FMM can be reduced to the appropriate limits of a Hookean solid, a Newtonian fluid and the classical Maxwell Viscoelastic fluid.

The fitting of the FVF and FMM models to the rheological data obtained for an HDPE, evidenced the ability of the fractional viscoelastic models to provide better results with a small number of parameters.

Numerical methods to solve simple unidirectional time-dependent shear flows with the three studied models were also described and verified with existing analytical solutions available in the literature. The results provided show that with these numerical approaches it is possible to deal both with fast transients and steady shear flows. The code has adaptive time stepping and can simulate for $0 \le t/\tau \le 1000$. However, due to the amount of information that has to be handled, the numerical calculation process is quite heavy, especially for the Fractional K-BKZ model, which is frame invariant. Consequently, improvements are required to be able to use those numerical approaches in more general calculation frameworks.

ACKNOWLEDGMENTS

L.L. Ferrás and J.M. Nóbrega would like to thank the funding by FEDER through the COMPETE 2020 Programme, the National Funds through FCT - Portuguese Foundation for Science and Technology under the project UID/CTM/50025/2013. L.L. Ferrás would also like to thank the funding by FCT through the scholarship SFRH/BPD/100353/2014. M.L. Morgado would like to thank the funding by FCT through Project UID/MAT/00013/2013 and M. Rebelo would also like to thank the funding by FCT through Project UID/MAT/00297/2013 (Centro de Matemática e Aplicações).

REFERENCES

1. I. Podlubny, *Fractional differential equations: an introduction to fractional derivatives, fractional differential equations, to methods of their solution and some of their applications* (Academic press, 1998).
2. A. Jaishankar, G.H. McKinley, Journal of Rheology **58** 1751-1788 (2014).
3. R.B. Bird, R.C. Armstrong, O. Hassager, Dynamics of Polymeric Liquids. Fluid Mechanics, second ed., (Wiley, 1987).
4. B. Keshavarz, T. Divoux, S. Manneville, G.H. McKinley, accepted for publication in Physical Review Letters (2016).
5. T.S.-K. Ng, G.H. McKinley, M. Padmanabhan, Appl Rheol **16** 265-274 (2006).
6. M. Caputo, Geophys. J. Int. **13** 529-539 (1967).
7. H. Schiessel, R. Metzler, A. Blumen, T.F. Nonnenmacher, Journal of physics A: Mathematical and General **28** 6567-6584 (1995).
8. C. Friedrich, Rheologica Acta **30** 151-158 (1991).
9. H. Schiessel , A. Blumen, J- Phys. A: Math. Gen. **26** 5057-5069 (1993).
10. G.W.S Blair, B.C. Veinoglou, J.E. Caffyn, Proceedings of the Royal Society A: Mathematical, Physical and Engineering Sciences **189** 69–87 (1947).
11. R. C. Koeller, J. Appl. Mech. **51** 299-307 (1984).
12. R.B. Bird, R.C. Armstrong, O. Hassager, *Dynamics of polymeric liquids Vol. 1: Fluid mechanics* (New York, Wiley, 1987).
13. P. Yang, Y. Cheong Lam, K.-Q. Zhu, J. Non-Newt. Fluid Mech. **165** 88-97 (2010).
14. A. D. Freed, K. Diethelm, Biomechan Model Mechanobiol **5** 203–215 (2006).
15. B. Bernstein, E. A. Kearsley, L.J. Zapas, Transactions of The Society of Rheology **7** 391–410 (1963).
16. M. H. Wagner, Rheologica Acta **15** 136–142 (1976).
17. M. H. Wagner, T. Raible, and J. Meissner, Rheologica Acta **18** 427–428 (1979).
18. R. G. Larson, *Constitutive Equations for Polymer Melts and Solutions* (Butterworths, Boston, 1988).
19. D. D. Joseph, International Symposium on Viscoelastic Fluids, Tobago,West Indies,1994.

20. M. Ansari, S.G. Hatzikiriakos, E. Mitsoulis, J. Non-Newtonian Fluid Mech. **167-168** 18–29 2012.
21. E. Mitsoulis, International Scholarly Research Notices - Polymer Science 2013 (2013).
22. T. Papanastasiou, G. Georgiou, A.N. Alexandrou, *Viscous fluid flow*, (CRC Press, 1999).
23. L.L. Ferrás, N.J. Ford, M.L. Morgado, M. Rebelo, G.H. McKinley, J.M. Nóbrega (submitted to Applied Mathematical Modelling).
24. E.A.J.F. Peters, M.A. Hulsen, B. H. A. A. van den Brule, J. Non-Newtonian Fluid Mech. **89** 209-228 (2000).
25. L.L. Ferrás, N.J. Ford, M.L. Morgado, M. Rebelo, G.H. McKinley, J.M. Nóbrega (to be submitted to Applied Mathematical Modelling).